Marine Structures 77 (2021) 102939

Contents lists available at ScienceDirect

Marine Structures

journal homepage: http://www.elsevier.com/locate/marstruc

Environmental lumping for efficient fatigue assessment of large-diameter monopile wind turbines

George Katsikogiannis *, Stian Høegh Sørum, Erin E. Bachynski, Jørgen Amdahl

Centre for Autonomous Marine Operations and Systems, Department of Marine Technology, Norwegian University of Science and Technology, Trondheim, NO-7491, Norway

ARTICLE INFO

Keywords:
Offshore wind turbines
Fatigue design
Environmental lumping
Aero-hydro-servo-elastic
Non-linear soil-structure interaction
Damage-equivalent contour lines

ABSTRACT

Fatigue damage is one of the governing factors for the design of offshore wind turbines. However, the full fatigue assessment is a time-consuming task. During the design process, the site-specific environmental parameters are usually condensed by a lumping process to reduce the computational effort. Preservation of fatigue damage during lumping requires an accurate consideration of the met-ocean climate and the dynamic response of the structure. Two lumping methods (time-domain and frequency-domain) have been evaluated for a monopile-based 10 MW offshore wind turbine, both based on damage-equivalent contour lines. Fatigue damage from lumped load cases was compared to full long-term fatigue assessment. The lumping methods had an accuracy of 94–98% for the total long-term fatigue damage and 90% for individual wind speed classes, for aligned wind and waves. Fatigue damage was preserved with the same accuracy levels for the whole support structure. A significant reduction of computational time (93%) was achieved compared to a full long-term fatigue assessment. For the cases with 30° and 60° wind-wave misalignment, there was a mean underestimation of approximately 10%. Variations in penetration depth did not affect the selection of the lumped sea-state parameters. This work presents a straightforward method for the selection of damage-equivalent lumped load cases, which can adequately preserve long-term fatigue damage throughout the support structure, providing considerable reduction of computational effort.

1. Introduction

Approximately 82% of all installed substructures for offshore wind farms in Europe employ monopile foundations [1]. It is expected that the monopile will remain the preferred choice due to manufacturing and fabrication experience [2]. Even with the introduction of higher capacity (8–12 MW) offshore wind turbines (OWTs), large-diameter monopiles are considered one of the most promising concepts for the future.

The design of monopile OWTs relies on dynamic analyses, coupling aerodynamics, hydrodynamics, soil-structure interaction and the wind turbine control system. Fatigue is one of the governing factors for the final design. Various methods can be applied for estimating the dynamic response and fatigue damage of offshore structures [3]. The results are sensitive to factors such as environmental load models, soil-structure interaction and statistical uncertainties. Time-domain simulations are considered the most accurate

* Corresponding author.
E-mail addresses: george.katsikogiannis@ntnu.no (G. Katsikogiannis), stian.h.sorum@ntnu.no (S.H. Sørum), erin.bachynski@ntnu.no (E.E. Bachynski), jorgen.amdahl@ntnu.no (J. Amdahl).

https://doi.org/10.1016/j.marstruc.2021.102939
Received 7 April 2020; Received in revised form 22 September 2020; Accepted 3 December 2020
Available online 11 February 2021

approach for fatigue damage estimation [4], because non-linear effects and coupling between environmental loads and structural responses are taken into account. However, fatigue assessment based on fully-integrated time-domain analyses is a time-consuming process, as all relevant combinations of environmental parameters should be considered. This includes joint occurrence of wind speed (U_w), significant wave height (H_s), wave peak period (T_p) and wind-wave directionality. Therefore, it is highly beneficial to reduce the number of environmental conditions considered for fatigue limit state (FLS) design. The challenge is to select a reduced set of load cases which accurately predicts the fatigue damage at all locations along the tower and monopile over the lifetime of the structure.

Lumping approaches from oil & gas industry, such as block lumping methods [5,6], cannot be applied for OWTs because they do not account for wind-wave correlation. Different lumping methods have been developed and applied for fatigue design of OWTs, such as Kühn's iterative damage-equivalent method [7], and Seidel's spectral energy-equivalent approach [8,9]. Still, design guidelines [10, 11] lack recommendations for how this should be performed.

Passon & Branner [12] showed that environmental lumping methods need to capture the OWTs' dynamics. The same study [12] introduced a new damage-equivalent lumping method for waves. This method preserves the wave-induced damage better than the probability-based averaging of sea-state parameters [13], Kühn's [7], and Seidel's [8,9] approaches. Passon & Branner also demonstrated the accuracy of the different lumping methods and their sensitivity to variation of different input parameters. Passon [14] extended the damage-equivalent wave lumping method to include wind-wave correlations. Lumped sea-state parameters are determined for each wind speed, wind direction and wave direction using damage-equivalent contour lines at selected positions within the OWT. The method was applied to a generic OWT configuration for a large-diameter (>8 m) monopile foundation. It was shown that the resulting lumped sea-states can accurately reproduce the long-term fatigue damage. However, several simplifications were introduced: the rotor-nacelle-assembly was modelled by a simplified mass-equivalent representation of the NREL 5 MW turbine [15] and only hydrodynamically induced fatigue damage was considered. Wind loads and aerodynamic damping were disregarded. This non-operational condition resembles design load case 7.2 [10], which typically only corresponds to 5% of a turbine's operational life [16].

To the authors' knowledge, the performance of Passon's method under simultaneous wind-wave loading has not been documented. Assessing this is important for a coupled system like OWTs. The present study develops and investigates the suitability of the damage-equivalent contour line lumping method for a 10 MW monopile-based OWT in operational conditions. Wind- and wave-induced responses are considered in an integrated manner. A frequency-domain lumping method for establishing the damage-equivalent contour lines and lumped load cases is developed. This is based on wave-induced dynamic responses. The resultant contour lines and load cases are compared to those obtained from a time-domain lumping method, which accounts for simultaneous dynamic wind and wave loads. The frequency-domain scheme is also evaluated for misaligned wind and waves.

To evaluate the accuracy of the lumping methods, the fatigue damage from the lumped load cases is calculated for combined wind and wave loads. The damage along the support structure compares well with results from full long-term fatigue damage assessment. Finally, the sensitivity of the selected lumped load cases to sea-state parameter variations and design changes, such as foundation characteristics, is examined. These topics have not been addressed before, and some of them were recommended by Passon [14] for further investigation. The proposed method predicts the long-term fatigue damage with high accuracy throughout the support structure while reducing the computation effort significantly compared to a full long-term analysis. This can be of great importance in the early design phase or for evaluating various types of modelling uncertainties, e.g. for different OWT design positions within a wind farm.

The paper is organized as follows: in section 2 a detailed description of the damage-equivalent lumping process and the lumping methods considered in the study is given, section 3 describes the environmental conditions, simulation and environmental load models, and section 4 gives all relevant information about fatigue damage calculations in the study. Finally, section 5 summarizes the results and section 6 concludes the paper with recommendations for future work.

2. Fatigue damage-equivalent lumping process

The full wind-wave climate used for OWT design is typically represented by wind speed-dependent scatter diagrams. Each wind speed class $k = 1, \ldots, N_{U_w}$ is usually associated with the mean wind speed at hub height, $U_{w,k}$, and a wind speed-dependent scatter diagram, SD_k. Each scatter diagram consists of N_{H_s} classes for significant wave height (H_s) and N_{T_p} classes for spectral peak period (T_p). The scatter diagrams contain the probability of occurrence, $p_{i,j,k}$ for wind speed class k, wave height class i and peak period class j. This results in a large number of load cases to be analysed for fatigue damage assessment. The computational effort required for fully-integrated time-domain analysis of so many load cases is significant. The lumping process aims to determine a reduced set of load cases, which represents the full wind-wave climate and predicts the correct fatigue damage.

2.1. Establishment of damage-equivalent contour lines

The selection of lumped sea-states is based on the damage-equivalent contour line method, as described by Passon [14]. Damage-equivalent contour lines (also referred as contour lines) refer to combinations of H_s and T_p that result in the same damage level at a given location along the structure. The basis of the method is to find $H_s - T_p$ combinations along these contour lines that can reproduce the total fatigue damage for a given wind speed class scatter diagram (SD_k). By finding the intersection of damage-equivalent contour lines from different locations along the support structure, a single $H_s - T_p$ combination for the lumped

sea-state can be found.

The first step to determine the contour lines is to calculate the unit damage $d^*_{i,j,k}$ for each sea-state in SD_k. This represents the fatigue damage for a specified time period with stationary environmental conditions, typically 1 h. The unit damages $d^*_{i,j,k}$ for selected locations along the OWT support structure are obtained either from fully-integrated time-domain analyses (subsection 2.2) or from a frequency-domain approach (subsection 2.3). The actual fatigue damage $d_{i,j,k}$ for each $H_s - T_p$ combination in SD_k is calculated by scaling the unit damage $d^*_{i,j,k}$ with the probability of occurrence $p_{i,j,k}$, according to Eq. (1). This follows from Palmgren-Miner's linear damage accumulation hypothesis [3,11].

$$d_{i,j,k} = p_{i,j,k} \cdot d^*_{i,j,k} \tag{1}$$

To establish the damage contour line, the target damage level d_{t_k} and target probability p_{t_k} are introduced. As shown in Eq. (2), d_{t_k} represents the total fatigue damage of all sea-states in SD_k, while p_{t_k} is the total probability of occurrence of SD_k.

$$d_{t_k} = \sum_{i=1}^{N_{Hs}} \sum_{j=1}^{N_{Tp}} d_{i,j,k} \quad \text{and} \quad p_{t_k} = \sum_{i=1}^{N_{Hs}} \sum_{j=1}^{N_{Tp}} p_{i,j,k} \tag{2}$$

The unit damages $d^*_{i,j,k}$ are now scaled by the probability p_{t_k} to obtain the scaled damages $d^*_{Si,j,k}$, according to Eq. (3). $d^*_{Si,j,k}$ represents the fatigue damage that will be predicted if $H_{s,i}, T_{p,j}$ is selected as the lumped load case for wind speed class k.

$$d^*_{Si,j,k} = p_{t_k} \cdot d^*_{i,j,k} \tag{3}$$

The intersection between $d^*_{Si,j,k}$ and d_{t_k} forms the damage contour line of the $H_s - T_p$ combinations that result in the target damage d_{t_k}. An example is shown in Fig. 1 for wind class 16–18 m/s. The multi-coloured surfaces represent the scaled damages $d^*_{Si,j,k}$ and the pink plane is the target damage level d_{t_k}. Each location along the OWT support structure has different response characteristics, resulting in different damage-equivalent contour lines. Therefore, damage equivalency throughout the whole support structure can only be maintained for sea-states that lie on the damage-equivalent contours for all locations. This will be discussed in detail in Secs. 2.2 and 2.3.

In the present study, two methods for establishing the damage-equivalent contour lines have been considered, based on time-domain and frequency-domain calculations. The steps described above are followed for both methods, with the difference being how the unit damage $d^*_{i,j,k}$ is calculated. The time-domain lumping method, described in subsection 2.2, serves as a validation of the frequency-domain lumping method. It uses fully-integrated analyses to account for simultaneous wind and wave excitation. Because $d^*_{i,j,k}$ shall be calculated for all possible sea-states in each wind speed class (including those with zero probability of occurrence), the computational effort is actually larger than that of a full long-term fatigue analysis. The frequency-domain lumping method (subsection 2.3) reduces the computational effort. Here, the unit damage $d^*_{i,j,k}$ is calculated based on a transfer function relating stress range to wave elevation.

After selecting the lumped sea-states, fully-integrated time-domain analyses are conducted for the reduced load set and the fatigue damage is compared to full scatter analysis results. Fig. 2 shows an overview of the methods used in the study for the fatigue damage calculation.

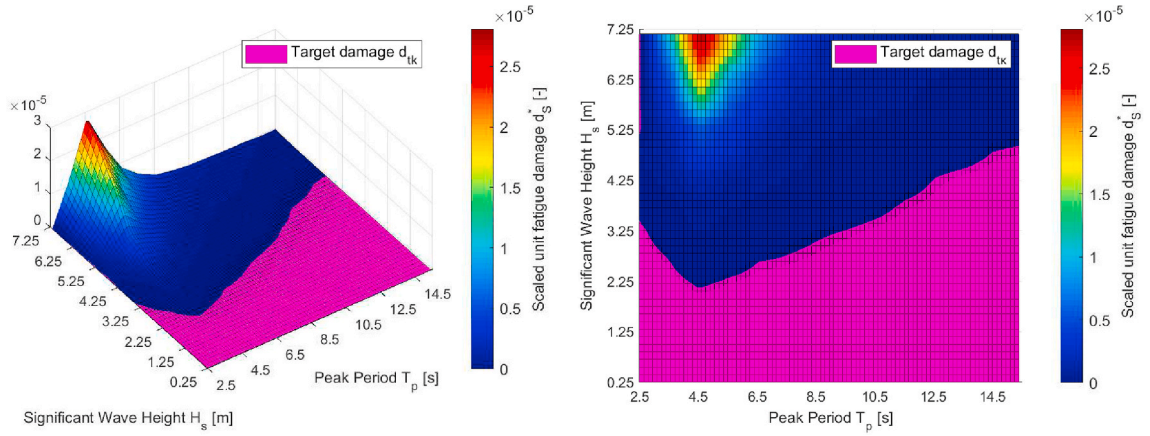

Fig. 1. Scaled damage $d^*_{S_k}$ (multi-coloured surface) and target damage level d_{t_k} (pink plane) for determining damage contour lines at mudline for wind speed class 16–18 m/s. (For interpretation of the references to colour in this figure legend, the reader is referred to the Web version of this article.)

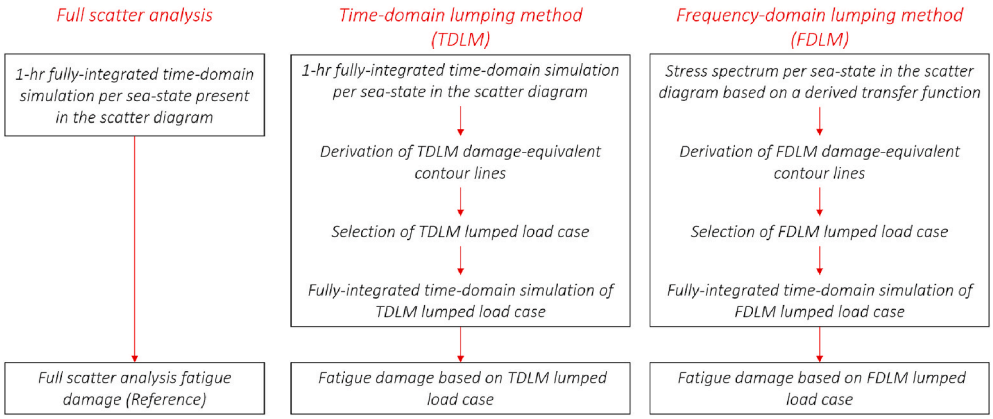

Fig. 2. Overview of lumping methods and full scatter analysis procedure for fatigue damage calculation in a single wind speed class.

2.2. The time-domain lumping method

The time-domain lumping method uses fully-integrated dynamic analyses to determine the damage-equivalent contour lines. The OWT is subjected to simultaneous turbulent wind and irregular wave excitation, and one analysis is conducted for each $U_w - H_s - T_p$ combination. The duration of each stochastic realisation is 1 h, following the recommendations of design standards [10,11]. The responses from the dynamic analyses are extracted at selected locations along the OWT and the fatigue damage is estimated using the rainflow cycle counting method, as shown in Fig. 3.

From the simulations, the unit ($d^*_{i,j,k}$) and actual ($d_{i,j,k}$) fatigue damage for each sea-state are established. The target fatigue damage d_{t_k} (Eq. (2)) varies along the support structure, resulting in different damage-equivalent contour lines for each location. Therefore, different $H_s - T_p$ combinations are required to achieve the target fatigue damage d_{t_k} for each location, and damage equivalency throughout the whole support structure can only be maintained for certain $H_s - T_p$ combinations. Having established the damage contour lines for several locations, a lumped load case can be determined by their intersection and used to represent the whole SD_k. This is illustrated in Fig. 4, where the contour lines for various locations along the monopile (red lines) and tower (blue lines) are shown for two wind speed classes. The lines vary, as each line represents a target fatigue damage that is usually different for different locations. However, they approximately intersect at one point. This $H_s - T_p$ combination (represented by the green circle) is considered the lumped sea-state for which long-term damage equivalency can be maintained along the support structure.

2.3. The frequency-domain lumping method

The frequency-domain approach seeks to extract the damage-equivalent contours in a simplified manner, based solely on wave loads. This is done using stress transfer functions, $H_{\zeta\sigma}$, relating wave elevation to stress range. Each wind speed class has its own transfer function because the soil stiffness and damping are influenced by the mean aerodynamic thrust, while the aerodynamic damping depends on the operating point of the turbine.

In this study, the transfer functions are extracted by subjecting the non-linear time-domain model of the OWT to frequency-limited 3-hr white noise wave excitation. A linear relationship is then assumed between the wave excitation and stress response of the OWT, yielding the transfer function as

$$H_{\zeta\sigma}(f) = \sqrt{\frac{S_{\sigma\sigma}(f)}{S_{\zeta\zeta}(f)}} \tag{4}$$

Here, $S_{\sigma\sigma}(f)$ is the power spectral density of the stress response, and $S_{\zeta\zeta}(f)$ is the incident wave spectrum. This is repeated for all wind classes.

Frequencies between 0 Hz and 0.7 Hz are included in the white noise wave spectrum, to include all relevant response frequencies. The significant wave height of white noise excitation is chosen as the mid value of the most probable H_s class in the scatter diagram for each wind speed. MacCamy & Fuchs' load model [18] is used in the simulations, as the transfer functions should represent the whole range of T_p values in the scatter diagram. Aerodynamic damping and mean thrust are captured by subjecting the operational turbine to a constant, uniform wind field. Tower shadow effects are neglected to avoid aerodynamic excitation interfering with the transfer functions.

The stress spectra for each sea-state in a wind speed class are found by combining the stress transfer function, $H_{\zeta\sigma}$, with the design wave spectra. From this, the unit fatigue damages $d^*_{i,j,k}$ are calculated. Assuming the stress to be Gaussian distributed and narrow-banded, the closed-form formulation [19] based on a Rayleigh distribution for stress cycles is used to estimate unit fatigue damage. For broad-banded spectra, Dirlik's empirical equation is used [20]. The bandwidth of the spectrum is evaluated based on the

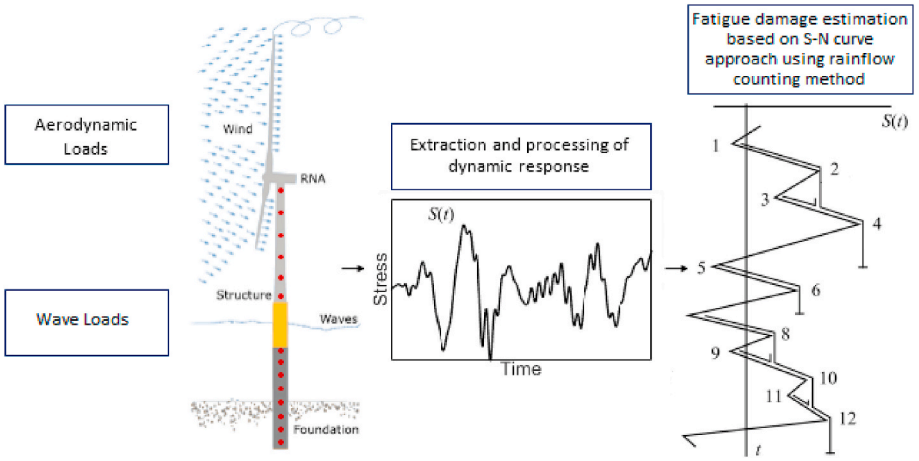

Fig. 3. Unit fatigue damage $d^{s}_{i,j,k}$ calculation per sea-state in time-domain lumping method for several locations (red dots) along a monopile-based OWT (monopile illustration [17], rainflow counting illustration [3]). (For interpretation of the references to colour in this figure legend, the reader is referred to the Web version of this article.)

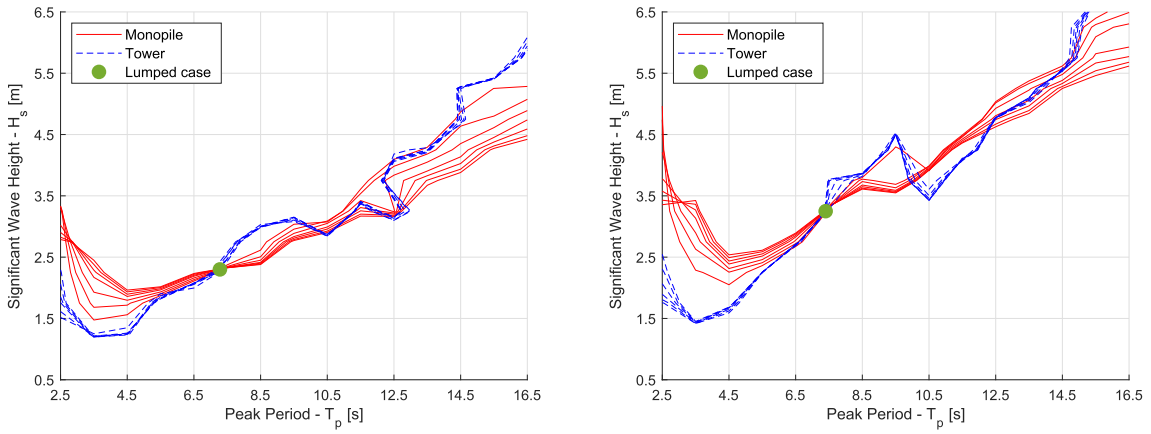

(a) Wind class 14-16 m/s **(b)** Wind class 18-20 m/s

Fig. 4. Damage-equivalent contour lines for various locations along the monopile and tower and the resultant lumped load case determined from time-domain lumping method.

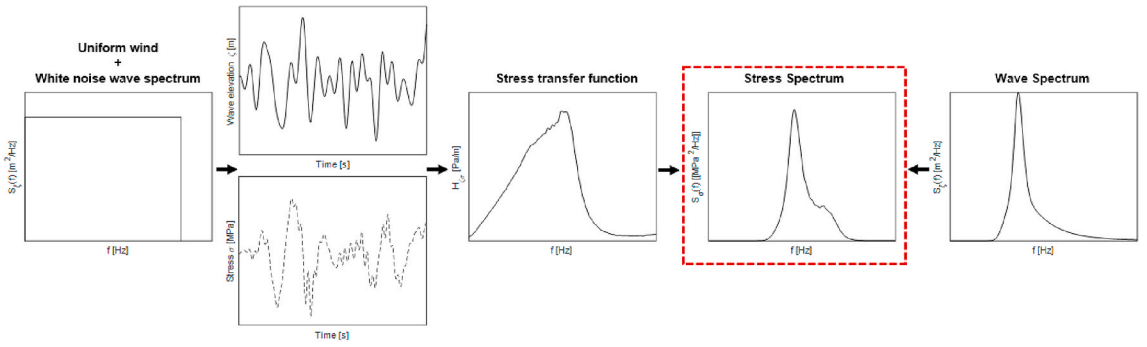

Fig. 5. Procedure for calculating wave-induced stress spectrum for each sea-state in a scatter diagram SD_k associated with wind speed class k for frequency-domain lumping method.

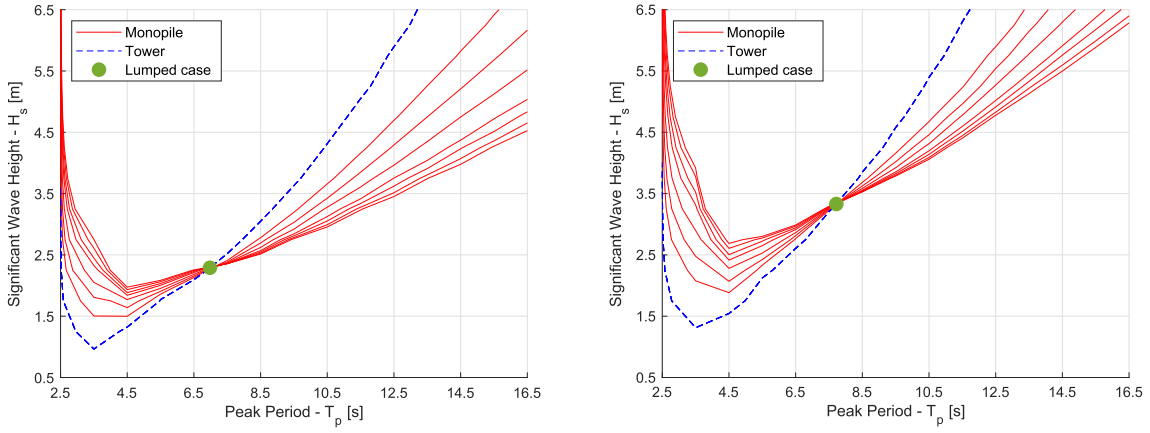

(a) Wind class 14-16 m/s **(b)** Wind class 18-20 m/s

Fig. 6. Damage-equivalent contour lines for various locations along the monopile and tower and the resultant lumped load case determined from frequency-domain lumping method.

bandwidth parameter $\beta = T_c/T_z$, where T_c is the mean period between peaks and T_z is the mean zero up-crossing period. Values of $\beta \geq 0.96$ indicate a narrow-banded spectrum [19]. Fig. 5 illustrates the steps for frequency-domain analysis. Once the unit fatigue damages are calculated, the lumping procedure proceeds as described in subsection 2.1.

Having determined the contour lines, the lumped load case can be found from their intersection, as illustrated in Fig. 6. It should be noted that the contour lines are for the same locations as in Fig. 4, but the contours are identical for all locations in the tower. This is further discussed in subsection 5.2, where the contour lines between the two lumping methods are compared.

The frequency-domain lumping method was also used for the wind-wave misalignment cases. In misaligned cases, the 3-hr white noise wave excitation is applied with the required misalignment angle, and the stress transfer function is extracted at the location on the cross section with the highest unit fatigue damage. Due to the low aerodynamic damping in the cross-wind direction, this position is in general not aligned with the wave direction (see subsection 5.4).

3. Environmental conditions and simulation models

This section will describe the model used in the case study, including environmental conditions, turbine properties and numerical modelling approaches.

3.1. Environment conditions - organization of environmental parameters

A numerical hindcast model from the National Kapodistrian University of Athens (NKUA) was used to generate 10-yr statistics for several locations in the North Sea, Atlantic Ocean and Mediterranean Sea for the Marina Platform project [21]. The hindcast data have a resolution of 1 h for the period 2001 to 2010 for a site located at the Norwegian Continental Shelf with geographic coordinates (55.11°N, 3.47°E) and 30 m water depth. The dataset provides information about met-ocean parameters such as mean wind speed (U_w) 10 m above sea level, significant wave height (H_s), wave peak period (T_p) and wind-wave directionality. The wind and wave roses of the site are shown in Fig. 7.

The wind speed U_{119} used in the study has been estimated at the hub height (119 m) of the wind turbine. Wind shear is accounted for by the power law with exponent $\alpha = 0.14$ [10]. A Kaimal wind spectrum with turbulence according to the normal turbulence model (NTM) for Class C turbines is used [10]. Current is not taken into account, as recommended by design standards [10].

The met-ocean data are expressed as 3D scatter diagrams of U_{119}, H_s and T_p. Wind speed classes in the operational range (4–25 m/s) have been considered, with classes of 2 m/s. For each wind speed, the corresponding sea-states are gathered in H_s classes of 0.5 m between 0.25 m and 9.25 m and T_p classes of 1 s in the range 2.5–16.5 s.

3.2. Simulation models

The simulation model is based on the DTU 10 MW reference wind turbine (DTU 10 MW RWT) [22], supported by a monopile foundation. The wind turbine has a hub height of 119 m relative to the MSL and a rotor diameter of 178.3 m. The rotor-nacelle assembly, tower and monopile above seabed were modelled in SIMO-RIFLEX, an aero-hydro-servo-elastic software developed by SINTEF Ocean. All wind inflow simulations were performed using TurbSim from NREL [23].

3.2.1. Wind turbine and support structure model

The wind turbine blades were modelled using the structural and aerodynamic coefficients from Ref. [22] and the controller adopted

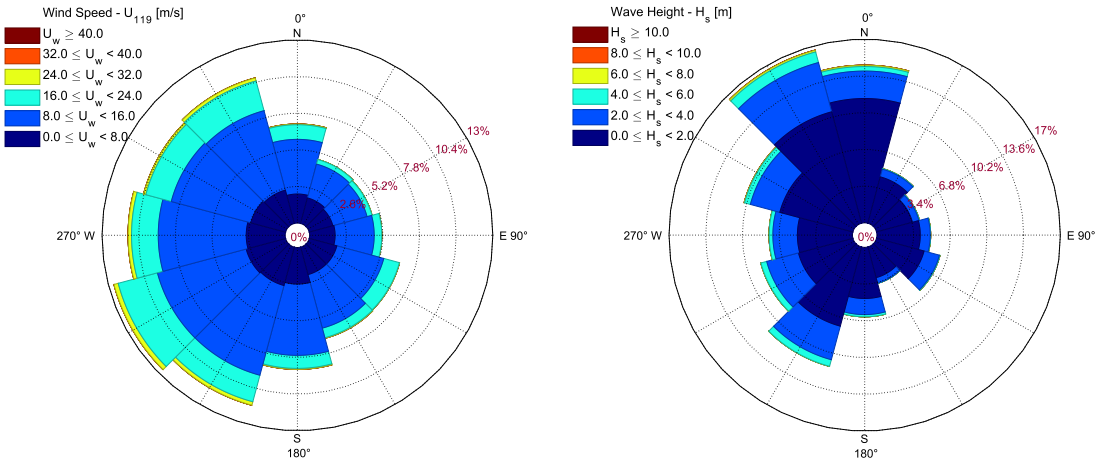

(a) Wind rose (b) Wave rose

Fig. 7. Site wind and wave roses based on the hindcast data.

was the basic DTU Wind Energy Controller [22]. Aerodynamic loads were calculated using the blade element momentum theory with engineering corrections such as the Glauert correction, Prandtl corrections for tip loss and hub loss [24], and dynamic stall and dynamic wake [25]. The tower was modelled with axisymmetric beam elements having 10 sections of constant diameter each, decreasing from a specified diameter at the bottom to the top of the tower. Similarly, the monopile was modelled with axisymmetric beam elements above seabed. The monopile part below seabed (foundation model) is described in detail in subsection 3.2.2.

3.2.2. *Foundation model*

A non-linear elasto-plastic model including hysteretic behaviour, based on the macro-element concept, was used for the foundation model. This type of model condenses the foundation and surrounding soil response to a force-displacement relation at one point, commonly located at mudline, separating the foundation and the rest of the structure [26].

This applied model predicts the load-displacement response and the hysteretic damping of monopile-based OWTs in integrated time-domain analyses [27]. The macro-element formulation is based on results from finite element analysis (FEA) of the soil and the foundation. The performance of the macro-element model was compared against field test measurements and FEA results for three piled foundations [17]. The model can reproduce the non-linear load-displacement response and the hysteretic behaviour observed in monopiles with different length-over-diameter ratios. Good agreement between the macro-element predictions and the FEA results confirms that the model can reproduce the soil-structure interaction with the same level of accuracy as the FEA, but with a considerable reduction in computational effort.

The macro-element model used in this study is calibrated to FEA results of full 3D continuum modelling of the soil volume and the foundation. The FE analysis considers a 3 m layer of sand and clay layers below. Tables 1 and 2 summarise the sand and clay layer properties respectively, used for the macro-element model calibration. The behaviour of the clay layers is represented by the NGI-ADP soil model [28], which describes the elasto-plastic, non-linear stress behaviour of saturated clays under undrained monotonic loading conditions. The model accounts for the effect of multi-directional loading, which has been found to affect the foundation stiffness and

Table 1
FEA soil parameters for sand layer (0–3 m), modelled with the hardening soil model.

Parameter	Value	Unit
Drainage type	Drained	–
Submerged weight, γ'	10	kN/m^3
Secant stiffness in standard drained triaxial test E_{50}^{ref}	3.0E+04	kPa
Tangent stiffness for primary oedometer loading, E_{oed}^{ref}	3.0E+04	kPa
Unloading and reloading stiffness, E_{ur}^{ref}	9.1E+04	kPa
Power for stress-level dependency of stiffness, m	0.54	–
Effective cohesion, C'_{ref}	1	kPa
Effective angle of internal friction, φ'_{ref}	34.25	deg
Angle of dilatancy, ψ	4.25	deg
Reference shear modulus at very small strains, G_0^{ref}	9.4E+04	kPa
Threshold shear strain at which $G_s = 0.722 \cdot G_0$, $\gamma_{0.7}$	0.015	%

Table 2
FEA soil parameters for clay layers (3–100 m), modelled with the NGI-ADP model.

Parameter	Unit	Depth [m]				
		3–9	9–18	18–36	36–72	72–100
γ'	kN/m^3	10	10	10	10	10
$G_{ur}/S_{u,A}$	–	1252	782.2	553.1	391.1	299.5
$\gamma_{f,C}$	%	10	10	10	10	10
$\gamma_{f,E}$	%	15	15	15	15	15
$\gamma_{f,DSS}$	%	15	15	15	15	15
$S_{u,ref}$	kPa	30	90	180	360	720
$S_{u,inc}$	kPa/m	10	10	10	10	10
$S_{u,P}/S_{u,A}$	–	0.48	0.48	0.48	0.48	0.48
$S_{u,DSS}/S_{u,A}$	–	0.67	0.67	0.67	0.67	0.67

- $G_{ur}/S_{u,A}$: Ratio of unloading/reloading shear modulus over active shear strength $\gamma_{f,C}$.
- $\gamma_{f,E}$, $\gamma_{f,DSS}$: Shear strain at failure in compression, extension, and direct simple shear (DSS) respectively.
- $S_{u,ref}$, $S_{u,inc}$: Active undrained shear strength at the top of each clay layer, and increase per meter.
- $S_{u,P}/S_{u,A}$: Ratio of passive shear strength over active shear strength.
- $S_{u,DSS}/S_{u,A}$: Ratio of DSS shear strength over active shear strength.

hysteretic damping [27]. The model communicates with SIMO-RIFLEX through a dynamic link library (DLL). The macro-element model does not directly compute the forces along the part of the pile embedded in the soil. A separate post-processing numerical tool has been employed to compute the moment distribution along the pile, developed by Norwegian Geotechnical Institute (NGI). A simplified illustration of the OWT model is shown in Fig. 8.

Five different monopile foundation designs have been used in this study. All models have a diameter (D) of 9 m and wall thickness (t) of 0.11 m. The base-case model has a penetration depth (L) of 36 m [29]. This is the model that is used to compare the fatigue damage from the derived lumped load cases to the full scatter results. The rest of the models, which vary in terms of penetration depth, are used to evaluate the sensitivity of the lumped load cases selection to foundation design. Table 3 summarizes the design properties of the models.

To quantify the natural frequency and damping of each foundation model, a free vibration analysis with no wind and no waves was conducted. The analysis was performed by gradually applying a force of 1.5 MN at the tower top and then releasing the force to allow the OWT to vibrate. Global damping was then quantified from the time history of the fore-aft bending moment at the mudline using the logarithmic decrement method, expressed in Eq. (5).

$$\delta = \ln\left(\frac{A_i}{A_{i+1}}\right) = 2\pi\frac{\xi}{\sqrt{1-\xi^2}} \approx 2\pi\xi \tag{5}$$

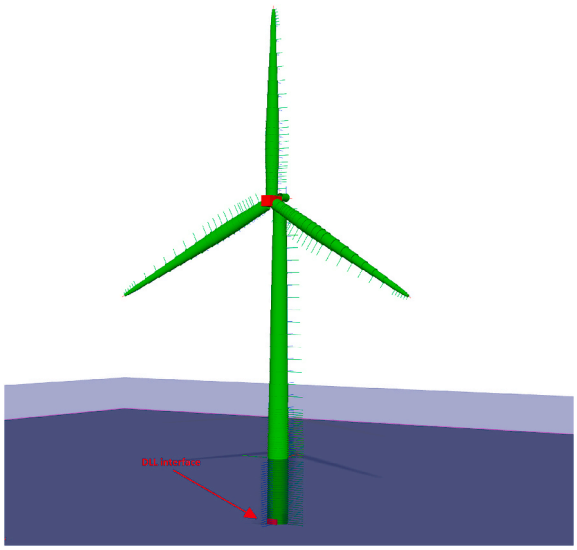

Fig. 8. Illustration of DTU 10 MW model in SIMO-RIFLEX.

Table 3
Foundation designs used in the study.

Foundation Model	Penetration Depth	L/D ratio	Monopile Diameter	Wall Thickness
[−]	[m]	[−]	[m]	[m]
1	22.5	2.5		
2	24.75	2.75		
3	27.0	3.0	9.0	0.11
(Base-case) 4	36.0	4.0		
5	45.0	5.0		

δ is the logarithmic decrement, A_i and A_{i+1} are two successive amplitudes and ξ is the global damping ratio estimate for that load cycle. Fig. 9 shows the first fore-aft natural frequencies of the support structure and the global damping ratios of the models, evaluated during the free decay tests. Higher load levels result in lower foundation stiffness and consequently in lower natural frequencies. In addition, the nonlinear damping is evident in the non-zero slope of the damping ratio with respect to response amplitude. This is clear for all the foundation models, which follow a steady behaviour from lower to higher response amplitudes.

3.2.3. *Wave load and wave kinematics models*

Two wave load models have been considered for the full scatter analysis, Morison's equation and MacCamy & Fuchs formulation [18] with Morison-type drag loads. Morison's equation cannot capture the diffraction effects important for low wave periods, but can be combined with wave kinematics of arbitrary order.

An estimate of the difference between the two models is found by considering the inertia loads on a rigid pile and calculating the wave load spectrum for several sea-states. Assuming a JONSWAP wave spectrum, the variance (σ^2) of the wave loads is determined for both models. The ratio $\sigma^2_{M\&F}/\sigma^2_{Mor}$ is used as a measure to identify the validity range of Morison's equation. Morison's equation is applied for sea-states where the difference between the two models is less than 5%. This corresponds to analyses with T_p higher than 10 s. The drag (C_D) and inertia (C_M) coefficients are assumed to be 0.9 and 2.0, respectively [30]. MacCamy & Fuchs formulation with Morison type drag is used for analyses with T_p lower than 10 s. The added mass coefficient related to the structural response is assumed to be constant and equal to 1.0 for the MacCamy & Fuchs hydrodynamic model.

Two wave kinematic theories have been considered for the full scatter analysis, Airy linear wave theory and Stokes' 2^{nd} order waves. Recommendations for wave models can be found in design guidelines when considering regular waves, but not for irregular waves [30]. To find the regions where 2^{nd} order wave theory is needed, the wave loads on a rigid monopile fixed at sea bed were compared. Linear wave theory with constant extrapolation of the wave potential up the instantaneous free surface was found sufficient for $H_s \leq$4.5 m. Second-order wave theory is used for higher sea-states. However, MacCamy & Fuchs load model is only valid for linear wave theory. Consequently, MacCamy & Fuchs with linear waves is used for analyses with H_s higher than 4.5 m and T_p lower than 10 s.

3.2.4. *Verification of frequency-domain modelling approach*

To verify the validity of the frequency-domain model, the stress spectra from the derived transfer functions were compared to stress spectra estimated from time-domain simulations. The three environmental conditions shown in Table 4 were used for the comparisons. Ten 1-hr simulations were conducted for each load case and the resultant stress spectra were averaged. Good agreement between the resulting stress spectra for the tower base and mudline is observed. This is shown in Fig. 10 for load case 2, while Table 5 compares the standard deviation for the load cases.

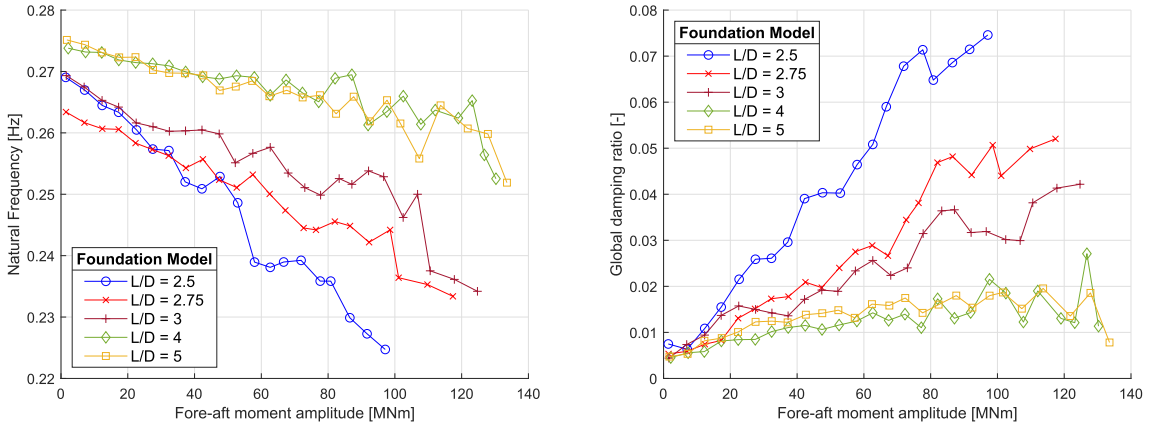

(a) Natural frequencies **(b)** Global damping ratios

Fig. 9. Dynamic properties of the foundation models from free-vibration test.

Table 4
Load cases for verification of frequency-domain approach.

Load Case	Wind Class	Mean Wind Speed	Significant Wave Height	Peak Period	Wave Spectrum
[−]	[m/s]	[m/s]	[m]	[s]	[−]
1	8–10	9.07	0.75	4.5	Pierson-Moskowitz
2	14–16	14.95	2.25	6.5	JONSWAP
3	18–20	20.91	3.25	7.5	JONSWAP

Further, it is desirable that no aerodynamic loads besides the mean thrust force and aerodynamic damping are present when establishing the transfer functions. By evaluating the variation in rotor speed and blade pitch, it was verified that the white-noise wave excitation does not significantly affect the operation of the turbine. For all wind speeds, the coefficient of variation was less than 0.5% for the rotor speed and the standard deviation of blade pitch angle was less than 0.07°.

4. Fatigue damage estimation

The time-domain simulations give the time history of loads at various cross sections along the monopile. These loads are denoted N_x (axial force), M_y and M_z (bending moments). Based on the coordinate system in Fig. 11, the axial stress σ_x at a given point (r, θ) on the outer surface of the tubular cross section with outer radius r is estimated as:

$$\sigma_x = \frac{N_x}{A} - \frac{M_y}{I_y} r\sin(\theta) + \frac{M_z}{I_z} r\cos(\theta) \tag{6}$$

Here, A is the cross-sectional area, I_y and I_z are the second moment of area for the cross section computed about the y and z axes, respectively. The shear stress and its resultant fatigue damage was not taken into account due to its negligible effect relative to the axial stress. The number of load cycles for different stress levels is computed based on rainflow counting technique [31] using the WAFO Toolbox [32], modified to allow for bi-linear S-N curves [33]. Representative S-N curves were selected based on DNV GL's recommended practice [4]. Curve "D" for steel in seawater with cathodic protection (Table 2.2 in Ref. [4]) was selected for the monopile, and curve "D" for steel in air (Table 2.1 in Ref. [4]) was selected for the tower. Since the fatigue damage is more pronounced in welds, S-N curves for girth welds were used [33]. A reference thickness equal to 25 mm and a thickness exponent on fatigue strength of 0.2 were used based on [4]. No stress concentration factor (SCF) is taken into account.

4.1. Long-term fatigue damage estimation

Three environmental models of increasing complexity have been utilised for comparing the long-term fatigue damage from the lumped load cases and the full scatter results. The first two models consider aligned wind and waves, while the third model accounts for wind-wave misalignment. It is assumed that the joint probability of all parameters can be expressed as the product of marginal and conditional probabilities [34]. The first model (model N°1) assumes aligned wind and waves without considering any directional variability. The probability of occurrence of an environmental condition is given by Eq. (7).

$$P_1\{U_{119}, H_s, T_p\} = P\{U_{119}\} P\{H_s, T_p | U_{119}\} \tag{7}$$

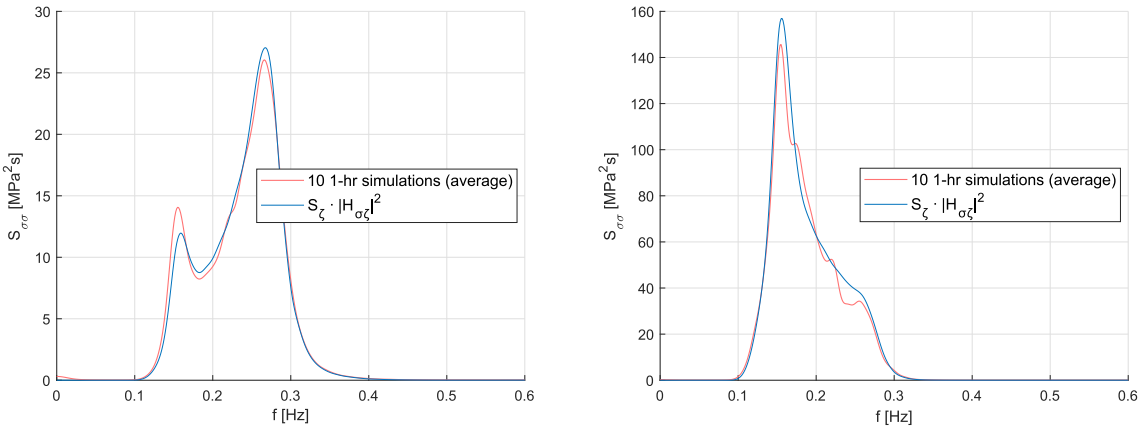

(a) Tower Base (b) Mudline

Fig. 10. Stress spectra comparison between the transfer function ($H_{\zeta\sigma}$) from the 3-hr white noise excitation and the actual wave spectrum (S_ζ) (basis of frequency-domain lumping method) and the averaged spectra of 10 1-hr time-domain simulations for load case 2.

Table 5
Standard deviation comparison from stress spectra of the sea-states used for the verification frequency-domain lumping method (FDLM).

Load Case	Mudline		Tower Base	
	$S_\zeta \cdot \lvert H_{\zeta\sigma}\rvert^2$ (Basis of FDLM)	1-hr simulations (Average)	$S_\zeta \cdot \lvert H_{\zeta\sigma}\rvert^2$ (Basis of FDLM)	1-hr simulations (Average)
[−]	Standard deviation [MPa]			
1	1.16	1.18	0.87	0.82
2	3.31	3.30	1.59	1.60
3	5.36	5.31	2.37	2.33

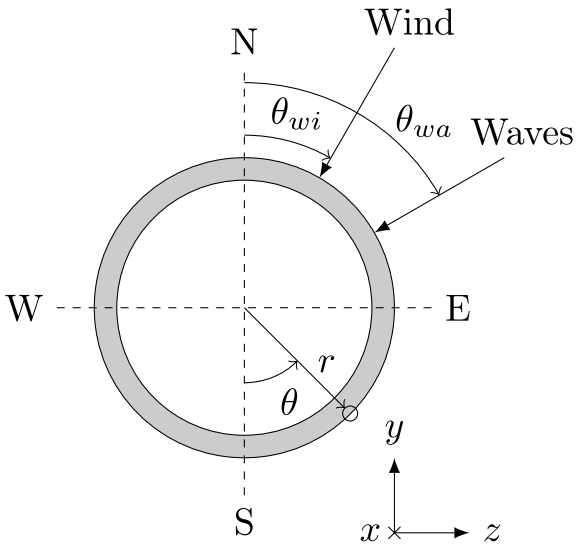

Fig. 11. Tubular cross-section local coordinate system and environmental parameters.

Long-term fatigue damage is calculated as the sum of the short-term (1 h) damage of each condition scaled by the probability of occurrence, by Eq. (8).

$$D_{LT_1} = 24 \cdot 365 \cdot N \cdot \sum_{k=1}^{N_{U_w}} \sum_{i=1}^{N_{H_s}} \sum_{j=1}^{N_{T_p}} d^*_{i,j,k} \cdot P_1\{U_{119}, H_s, T_p\} \tag{8}$$

Here, N is the design lifetime in years, $d^*_{i,j,k}$ is the 1-h fatigue damage, N_{U_w} is the number of wind speed classes, and N_{H_s}, N_{T_p} the number of H_s and T_p classes for a scatter diagram SD_k, associated with wind speed class k.

In the second model (model N^{o}2), long-term directional variability of wind is taken into account. Each wind speed class is divided into twelve sectors ($N_{\theta_{wi}}$), each covering an angle of 30°. The probability of occurrence of a sea-state and fatigue damage for this model are formulated by Eqs. (9) and (10)

$$P_2\{U_{119}, \theta_{wi}, H_s, T_p\} = P\{U_{119}\} P\{\theta_{wi} | U_{119}\} P\{H_s, T_p | U_{119}, \theta_{wi}\} \tag{9}$$

$$D_{LT_2} = 24 \cdot 365 \cdot N \cdot \sum_{k=1}^{N_{U_w}} \sum_{l=1}^{N_{\theta_{wi}}} \sum_{i=1}^{N_{H_s}} \sum_{j=1}^{N_{T_p}} d^*_{i,j,k,l} \cdot P_2\{U_{119}, \theta_{wi}, H_s, T_p\} \tag{10}$$

where θ_{wi} is the wind direction with respect to North.

Model N^{o}3 is an extension of the second model, taking into account wind-wave misalignment per wind speed class. When considering misaligned wind and waves, the hindcast does not contain enough data to accurately model the full joint probability distribution. Eqs. (11) and (12) are used for Model N^{o}3.

$$P_3\{U_{119}, \theta_{wi}, \theta_{rel}, H_s, T_p\} = P\{U_{119}\}P\{\theta_{wi}|U_{119}\}P\{\theta_{rel}|U_{119}\}P\{H_s, T_p|U_{wi}, \theta_{rel}\} \tag{11}$$

$$D_{LT_3} = 24 \cdot 365 \cdot N \cdot \sum_{k=1}^{N_{U_w}} \sum_{l=1}^{N_{\theta_{wi}}} \sum_{m=1}^{N_{\theta_{rel}}} \sum_{i=1}^{N_{H_s}} \sum_{j=1}^{N_{T_p}} d_{i,j,k,l,m} \cdot P_3\{U_{119}, \theta_{wi}, \theta_{rel}, H_s, T_p\} \tag{12}$$

Here, θ_{rel} is the absolute wind-wave misalignment angle in the interval $\theta_{rel} \in [0°, 180°]$. For all three models described, the wave climate $P\{H_s, T_p\}$ is represented as a conditional scatter diagram. By utilizing the symmetry of the monopile, the same simulation results can be used for all wind directions.

5. Results and discussion

The results section is ordered as follows. In subsection 5.1, the lumped load cases from the time-domain and frequency-domain methods are compared to the most probable and most damage contributing H_s, T_p classes from the full long-term analysis. In subsection 5.2, selected contour lines from the two lumping methods are compared for two different wind speed classes and their differences are discussed. In subsection 5.3.1, the uncertainty of fatigue damage prediction for the lumped load cases is evaluated. In subsection 5.3.2, the fatigue damage from the lumped load cases is compared to full scatter results for aligned wind and waves, and subsection 5.3.3 focuses on damage preservation along the support structure through the lumping process. In subsection 5.5, the damage sensitivity to variations in H_s and T_p values of the lumped load cases is discussed. In subsection 5.4, the frequency-domain lumping method is evaluated and compared to full scatter results for wind-wave misalignment conditions. Finally, subsection 5.6 focuses on the sensitivity of the resulting load cases from frequency-domain lumping method to different foundation designs, with varying penetration depth.

5.1. Lumped load cases compared to wind speed scatter diagrams

First, the sea-state parameters of the lumped load cases from time-domain (subsection 2.2) and frequency-domain (subsection 2.3) methods are compared. The lumped $H_s - T_p$ combinations, which represent the wind speed class scatter diagrams (SD_k), are also compared to the most probable H_s, T_p classes within each SD_k and to the H_s, T_p classes that resulted in the largest fatigue damage based on the full scatter analysis. The results are shown in Fig. 12 and Table 6.

Both methods result in similar H_s values (~0.1 m difference for most wind speed classes), following a gradual increase from low to high wind speeds, as expected. The slightly higher H_s values (~0.15–0.3 m) obtained by the frequency-domain lumping method close to the rated speed can be explained by the fact that in this wind speed range, the slowly-varying wind component dominates the dynamic response and consequently the fatigue damage [35]. This physical process is not taken into account during the frequency-domain lumping method, which then leads to higher values for the required H_s. Finally, the derived H_s values are similar to the most probable and most damage contributing H_s classes from the full scatter analysis results.

The two methods show a larger scatter regarding the T_p values of the lumped load cases. In most wind speed classes the differences in T_p are between 0.1 s and 0.5 s, without a specific trend above the rated speed. Below the rated speed, lower T_p values are obtained from the time-domain lumping method. Lower T_p counteracts the lower H_s values in that range as the decreased peak period leads to an larger number of load cycles per time, increasing the fatigue damage. Additionally, considering that the natural period of the structure

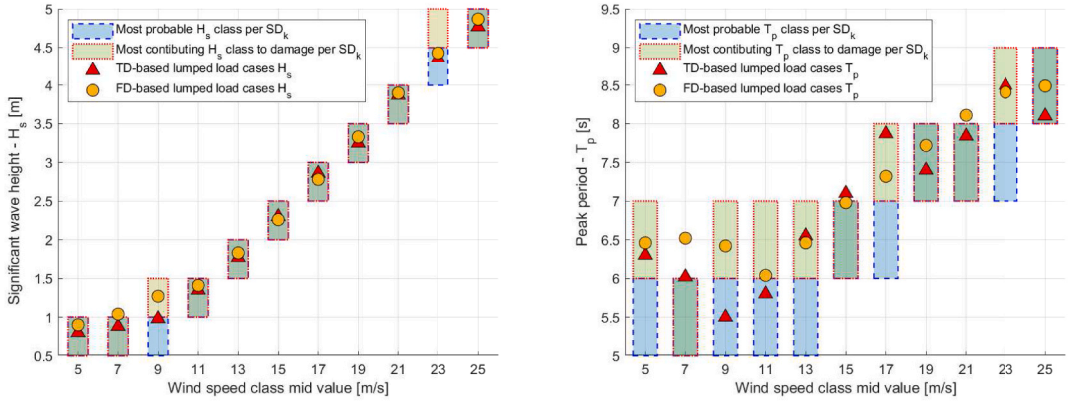

(a) Significant wave height per wind class

(b) Peak period per wind class

Fig. 12. Derived sea-state parameters $H_s - T_p$ of the lumped load cases compared to the most probable and most contributing sea-state parameters derived from the full scatter analysis (SD_k: Scatter diagram of wind class k, *TD*: Time-domain, *FD*: Frequency-domain).

Table 6
Summary of lumped load cases and sea-state parameters for each wind class.

Wind Class	H_s [m]				T_p [s]			
[m/s]	TDLC[a]	FDLC[b]	MPSD[c]	MCSD[d]	TDLC	FDLC	MPSD	MCSD
4–6	0.80	0.90	[0.5,1.0]	[0.5,1.0]	6.30	6.46	[5,6]	[6,7]
6–8	0.88	1.04	[0.5,1.0]	[0.5,1.0]	6.02	6.52	[5,6]	[5,6]
8–10	0.98	1.27	[0.5,1.0]	[1.0,1.5]	5.50	6.42	[5,6]	[6,7]
10–12	1.35	1.41	[1.0,1.5]	[1.0,1.5]	5.80	6.04	[5,6]	[6,7]
12–14	1.77	1.83	[1.5,2.0]	[1.5,2.0]	6.55	6.46	[5,6]	[6,7]
14–16	2.30	2.26	[2.0,2.5]	[2.0,2.5]	7.10	6.98	[6,7]	[6,7]
16–18	2.86	2.78	[2.5,3.0]	[2.5,3.0]	7.87	7.32	[6,7]	[7,8]
18–20	3.25	3.33	[3.0,3.5]	[3.0,3.5]	7.40	7.72	[7,8]	[7,8]
20–22	3.87	3.9	[3.5,4.0]	[3.5,4.0]	7.84	8.11	[7,8]	[7,8]
22–24	4.36	4.43	[4.0,4.5]	[4.5,5.0]	8.50	8.41	[7,8]	[8,9]
24–26	4.77	4.87	[4.5,5.0]	[4.5,5.0]	8.10	8.49	[8,9]	[8,9]

[a] TDLC: Lumped load case based on time-domain method.
[b] FDLC: Lumped load case based on frequency-domain method.
[c] MPSD: Most probable sea-state parameter class.
[d] MCSD: Most damage contributing sea-state parameter class (from full scatter analysis).

is approximately 3.85 s (Fig. 9a), a decreased peak period approaches the range of the support structure natural period. This leads to pronounced dynamic responses, increasing the fatigue damage.

5.2. Contour lines comparison between the lumping methods

The overall shape of the contour lines from the two lumping methods highlights the dynamic response of the support structure. This is indicated in Fig. 13 for two wind speed classes. For peak periods in the vicinity of the first natural period (3.7–4.0 s), resonance increases the fatigue damage. Low H_s values are then required to obtain the target damage value d_{t_k} for each location. For long wave periods, the response can be considered as quasi-static, and the increased peak period further decreases the number of load cycles per time. Therefore, a considerably higher H_s is required to obtain the target fatigue damage. A similar trend is observed for short wave periods; although the number of load cycles increases as a result of the decreased mean wave period, the dynamic amplification factor is low.

The contour lines from the time-domain lumping method show more irregular behaviour compared to those from frequency-domain and those found by Passon [14]. This is a consequence of how the unit damage $d^*_{i,j,k}$ is estimated for each sea-state in SD_k. In the time-domain method, $d^*_{i,j,k}$ is estimated using a single 1-hr realisation for each sea-state. The aleatory uncertainty in fatigue damage from a single 1-h realisation can be up to 25% depending on the location (as shown in subsection 5.3.1), leading to the irregular shape of the contour lines. The irregularities are pronounced for the contour lines that correspond to the tower, especially for wind classes below and close to the rated wind speed. This is because fatigue damage estimation for the tower is strongly affected by both the random wind and

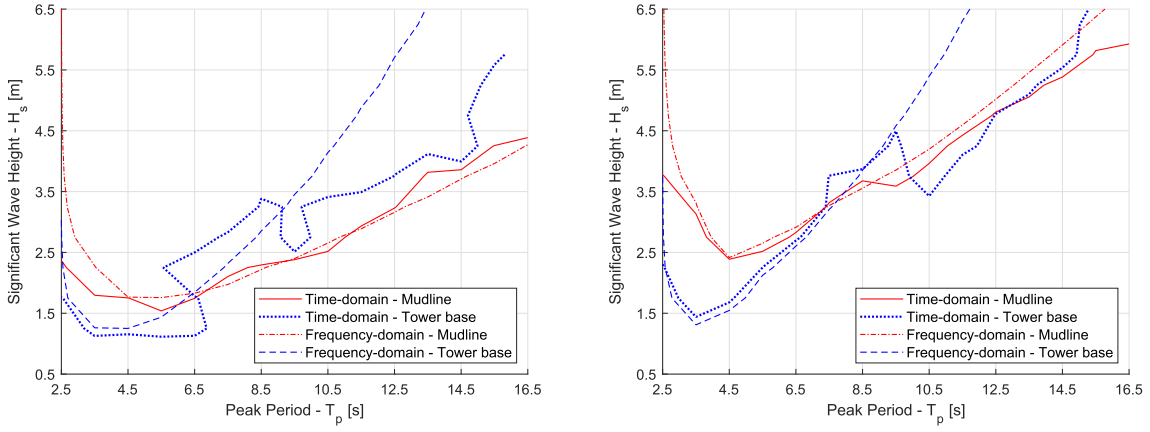

(a) 12-14 m/s (b) 18-20 m/s

Fig. 13. Contour lines from frequency-domain and time-domain lumping methods. The contours are shown for the monopile at mudline and tower base (11 m above sea-surface).

wave field of each realisation, while the monopile's dynamic response and resultant damage is dominated by the wave loading.

The monopile contour lines from the two methods align well for the whole range of $H_s - T_p$ combinations. As shown in Figs. 4 and 6, different locations in the monopile have different contour lines. This is caused by the total response being a combination of quasi-static and dynamic response. For the tower, the frequency-domain contours require larger H_s than the time-domain method for high T_p values. This is due to the lack of wind-induced responses in the frequency-domain lumping process. Further, the contour lines in Fig. 6 are identical for the tower, since the loads are only caused by the acceleration of the rotor-nacelle assembly. This is not the case for the time-domain lumping, where aerodynamic loads also contribute to the response. Nonetheless, the contours from the two methods align well for moderate sea-states, where the fatigue damage is dominated by the wave excitation and the pronounced dynamic responses close to the support structure first natural period.

Fig. 14 shows a comparison between the stress spectra obtained using the transfer functions of frequency-domain lumping method and the stress spectra of the same load cases subjected to combined fluctuating wind and irregular wave loading. At mudline, the main difference between the spectra is the low-frequency wind-induced response ($f < 0.1$ Hz) and the 3P rotor response, which are not present in the frequency-domain model. However, wave excitation is the main contributor to the fatigue damage. Therefore, the monopile contour lines of the two methods are in good agreement because wave loading is included in both lumping methods.

The tower base response is dominated by the slowly-varying wind components. Inertia loads from the RNA acceleration at the natural frequency (f_n) and the 3P rotor loads also contribute to the response. To compensate for the lack of the slowly-varying response due to wind excitation, the frequency-domain lumping method leads to higher H_s values than the time-domain method for large T_p. This effect is enhanced for wind classes close to the rated speed, where the contribution of wind-induced response to fatigue damage is relatively high.

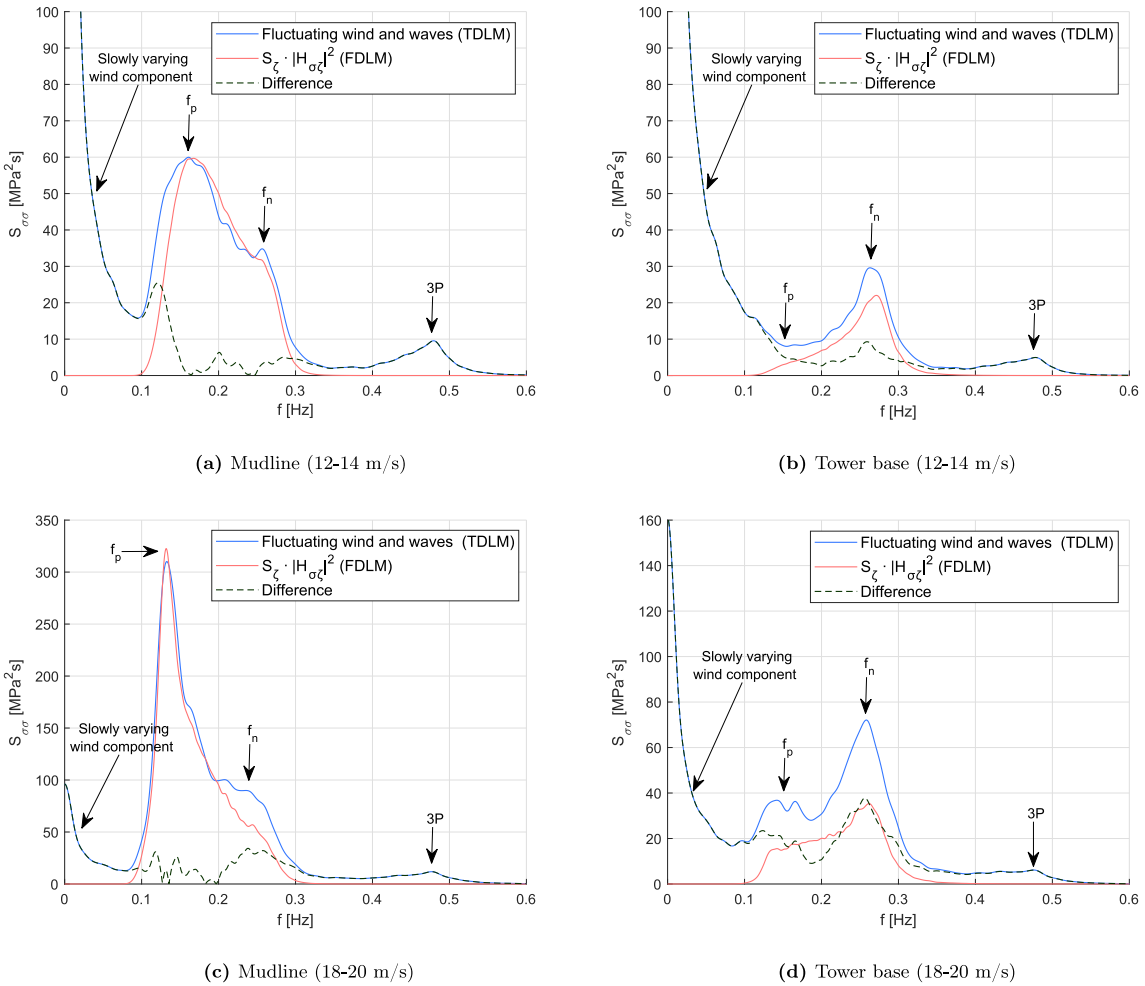

(a) Mudline (12-14 m/s)

(b) Tower base (12-14 m/s)

(c) Mudline (18-20 m/s)

(d) Tower base (18-20 m/s)

Fig. 14. Stress spectra from the frequency-domain lumping method (FDLM) using the transfer function $H_{\zeta\sigma}$ obtained based on uniform wind and 3-hr white noise wave loading, and from time-domain lumping method (TDLM) for combined wind-wave loading for the lumped load cases in wind class 12–14 m/s (top) and 18–20 m/s (bottom). f_p denotes the wave peak frequency, f_n is the support structure natural frequency and 3P is the blade passing frequency.

5.3. Fatigue damage comparison for aligned wind-waves

The assessment of a lumping method is based on the accuracy of the predicted damage from the lumped cases when compared to a full scatter analysis. To estimate the fatigue damage of the reduced load set, the OWT is subjected fully-integrated time-domain analyses with simultaneous turbulent wind and irregular wave excitation for the frequency-domain lumped load cases (Table 6 - FDLC). The time-domain lumped load cases (Table 6 - TDLC) have not been compared to full scatter results for two reasons. Firstly, because the lumped load cases from time- and frequency-domain methods are similar. Secondly, the time-domain lumping method is only used for comparison to frequency-domain method and not as an alternative to full scatter analysis because of its high computational effort.

5.3.1. Evaluation of damage estimation uncertainty by the lumped cases

The statistical uncertainty is expected to increase when a single environmental condition is used to represent all sea-states in a wind speed class. Therefore, several realisations of the same condition may be required to obtain accurate estimates of the fatigue damage. This is investigated by conducting 20 1-hr analyses for each lumped load case, with random wind and wave seed. The uncertainty is expressed by the coefficient of variation (C.o.V.) for a given number of seeds per sea-state. Fatigue damage is evaluated at the upwind position at mudline and at tower base. Fig. 15 shows the results for five selected wind speed classes. C.o.V. varies between approximately 4.5% and 24% for a single realisation, with a gradual reduction as the number of seeds increases.

For locations along the support structure where the wind contribution to fatigue damage is considerable, the estimated damage varies more. For example, in Fig. 15, the C.o.V. is larger at the tower base than at the mudline. Therefore, more analyses are required to achieve same level of C.o.V. For both locations, the C.o.V. is higher for wind classes close to the OWT rated speed (11 m/s), showing a maximum for class 8–10 m/s, while the lowest C.o.V. values are found for the highest wind speed class (24–26 m/s). By requiring a C.o.V. limit of 10% for the evaluation of the lumping method, five 1-hr time-domain analyses for each lumped load case are used for the comparisons with the full scatter results. This is considered a reasonable compromise between accuracy and computational effort.

5.3.2. Lumped load cases damage compared to full scatter results

This section will compare the long-term fatigue damage estimates obtained from the lumped load cases with the results from the full scatter analysis. This is first done assuming aligned wind and waves, corresponding to environmental models N^{o}1 and N^{o}2 in subsection 4.1. To evaluate the uncertainty caused by using five 1-h realisations of the lumped load cases, 4 “sets” of results are generated. Each set consists five 1-hr realisations of the 11 lumped load cases (Table 6 - FDLC) associated with the different wind speed classes. The average damage is used for the comparisons. A negative (positive) difference implies an underestimation (overestimation) of the damage calculated by the lumped set with respect to the full scatter result. The results are compared at the location along the monopile with the highest long-term fatigue damage, 8.25 m below the mudline. Fig. 16 shows the total and per wind class damage comparisons.

Although the four sets consist of identical lumped load cases in terms of environmental parameters, stochastic variation in the estimated fatigue damage is significant. The relative differences for individual wind speed classes for both models show a variation between approximately ±13% with respect to full scatter results as a consequence of seed variability. As an example, focusing on wind class 20–22 m/s in Fig. 16b, the damage difference ranges between 11% (Set N^{o}1) to −6.7% (Set N^{o}4) compared to the full scatter results. The total fatigue damage relative differences are however relatively stable, with the largest underestimation being

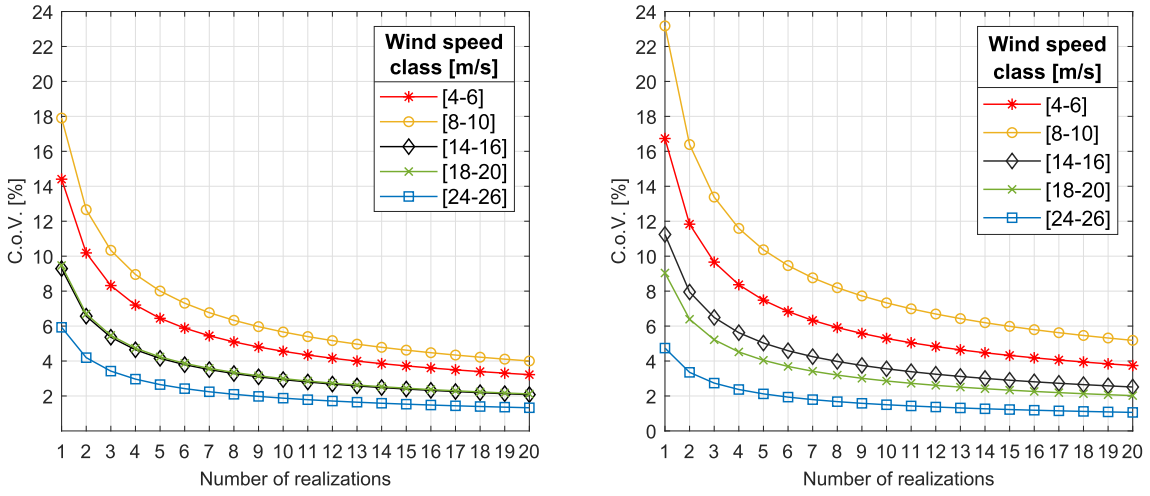

(a) Mudline (b) Tower Base

Fig. 15. Statistical uncertainty of fatigue damage estimation as a function of number of seed realisations for two locations along the support structure.

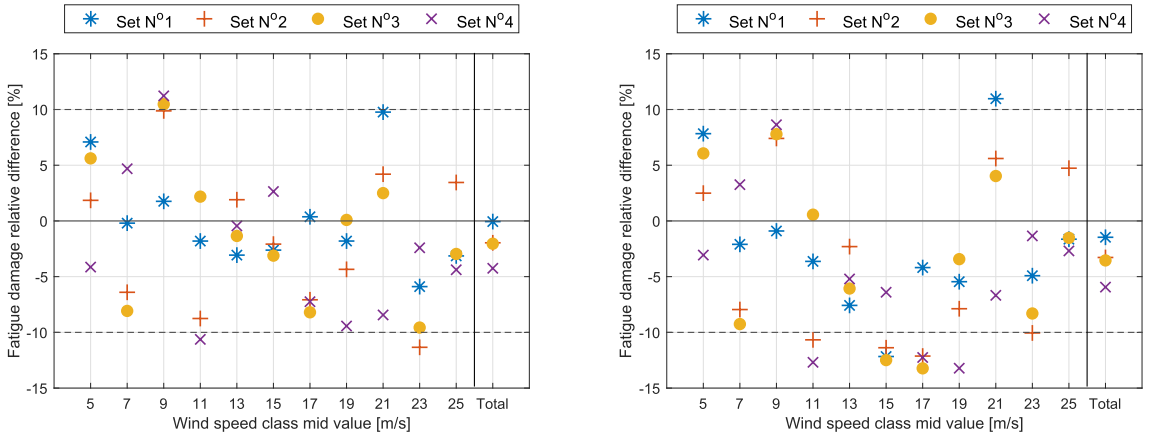

(a) Model N°1 (b) Model N°2

Fig. 16. Total and per wind class fatigue damage relative difference between lumped load cases per set and full scatter results for aligned wind and waves, without (Model N°1) and with (Model N°2) considering long-term wind direction variability. Comparison at the monopile location (vertical and around the circumference) with the highest long-term fatigue damage.

approximately 6%. The fatigue damage relative differences of models N°1 and N°2 compared to full scatter results show negligible variations, implying that the damage equivalency of the lumping method holds without and with considering long-term wind directional variability. Based on the above, using five realisations for each lumped load case results in acceptable variations in fatigue damage estimation per wind class. Finally, comparing Model N°1 and Model N°2, a significant reduction (~64%) of the total and per wind class fatigue damage was observed, due to the long-term wind directional variability, explained by the wind-wave roses in Fig. 7.

5.3.3. Fatigue damage equivalency along the OWT support structure

Several damage-equivalent contour lines along the monopile and tower were used, as described in section 2. The objective is to select a lumped load case for which the fatigue damage could be potentially preserved for the whole support structure. Fig. 17 confirms that this is achieved, using three wind speed classes for illustration. The lumped load cases can result in either underestimation or overestimation of the fatigue damage compared to full scatter results as shown in Fig. 16. Overall, the deviations are small, especially for the total fatigue damage, considering all the relevant uncertainties related to lumping process, fatigue calculation, and non-linearities.

The total fatigue damage preservation through the lumping process is also illustrated for three different cross sections along the support structure in Fig. 18, for environmental Model N°2. In addition, Fig. 19 shows the individual contribution to the total fatigue damage from each wind speed class for each cross section in Fig. 18. As noted in subsection 5.2, the fatigue damage in the tower is dominated by the responses due to wind loading close to the rated speed. This is indicated by the relatively high contribution of wind classes 6–8 m/s 10–12 m/s and 12–14 m/s in Fig. 19a. For locations in lower positions along the monopile, the wave loads gradually become more important for the fatigue damage.

5.4. Misaligned wind-wave conditions

The frequency-domain lumping method was also applied for wind-wave misalignment conditions. The same procedure is followed as described in subsection 2.3, except that the 3-hr white noise wave excitation is now applied with the required misalignment angle with respect to the uniform wind field, which is applied in the fore-aft direction. The stress transfer function is extracted at the location on the cross section with the highest unit fatigue damage.

With misaligned wind and wave conditions comes a difference in the direction of the primary excitation sources of an OWT. As a result, the maximum response will neither be aligned with the wind nor the wave direction. Further, the lack of aerodynamic damping in the cross-wind direction will increase the cross-wind response for the wave-only analyses [36]. This is illustrated in Fig. 20, where the lumped load case for wind class 18–20 m/s was simulated with fluctuating wind and waves and with uniform wind and waves. In both cases, wind is arriving from 0° (fore-aft direction) and waves are arriving from 30°. The difference between the locations with largest fatigue damage when considering and neglecting the turbulent wind excitation is approximately 35° in the tower base, i.e. larger than the wind-wave misalignment. This differs from the case with aligned wind and waves, and it is of interest to investigate the accuracy of the lumping method when considering wind-wave misalignment.

Three wind speed classes have been analysed to limit the computational effort. These are the wind speed classes 6–8, 12–14 and 18–20 m/s, which have been analysed for 30° and 60° wind-wave misalignment. Only the 30° results are presented here, as the results for the two misalignment angles are similar. Fig. 21 shows the maximum fatigue damage along the monopile and tower. The lumped load cases underpredicts the fatigue damage for all wind speeds. For the wind class 12–14 m/s, the error is 7% for the most critical

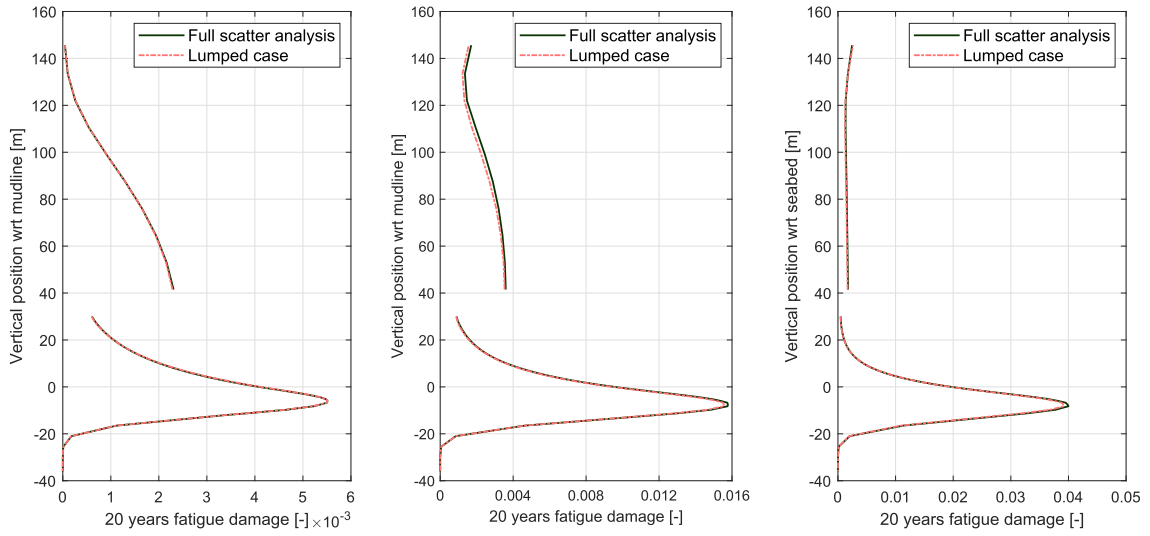

(a) Wind class 6-8 m/s (b) Wind class 12-14 m/s (c) Wind class 18-20 m/s

Fig. 17. Lifetime fatigue damage from full scatter diagram analyses and lumped load cases for aligned wind-waves (Model N^{o}1).

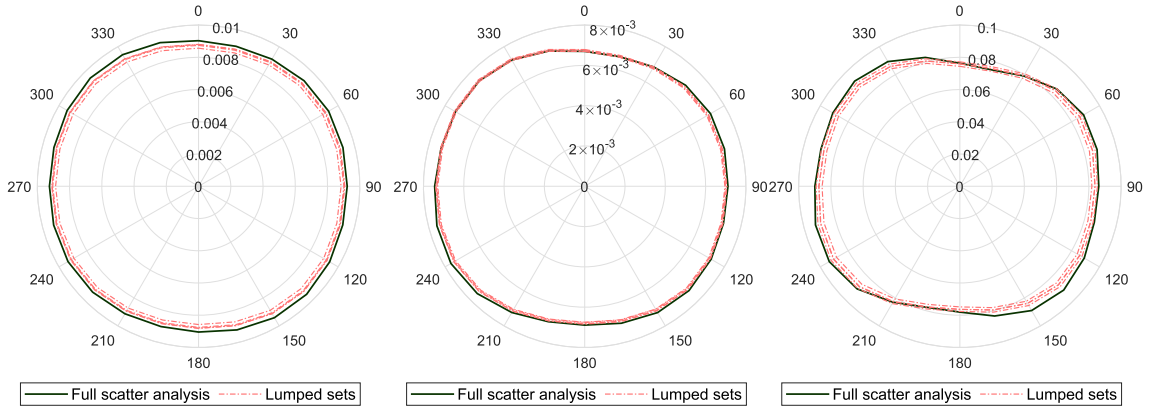

(a) Tower base (b) 15 m above mudline (c) 8.25 m below mudline

Fig. 18. Total fatigue damage for three different cross-sections along the support structure obtained from full scatter analysis and the 4 lumped load sets (Model N^{o}2).

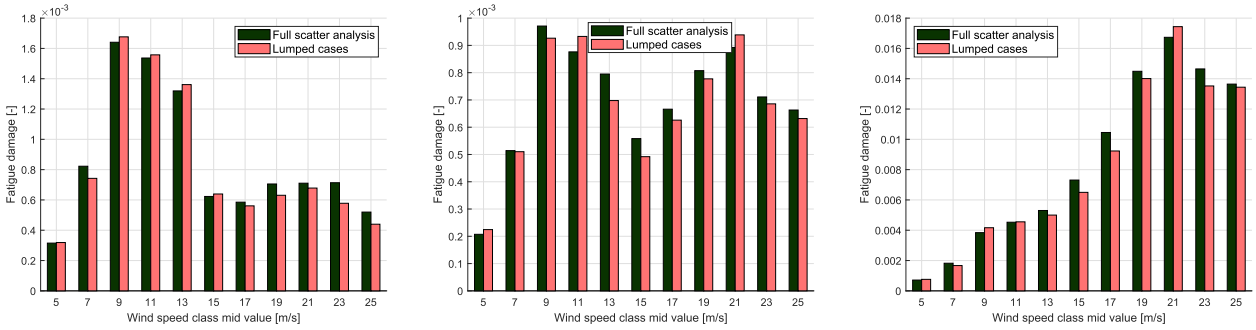

(a) Tower base (b) 15 m above mudline (c) 8.25 m below mudline

Fig. 19. Contribution of individual wind speed classes to total fatigue damage for the three cross-sections of Fig. 18 from full scatter analysis and a lumped load set (Model N^{o}2).

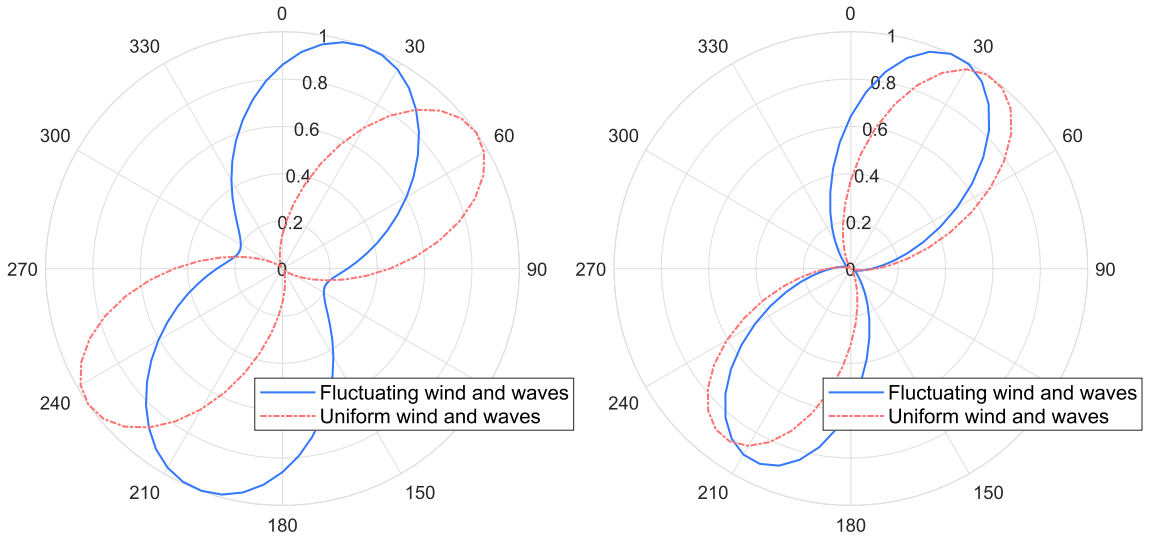

(a) Tower base (b) Mudline

Fig. 20. Normalised fatigue damage at tower base and mudline for lumped load case in wind class 18–20 m/s with 30° wind-wave misalignment. The mean wind direction is from 0°.

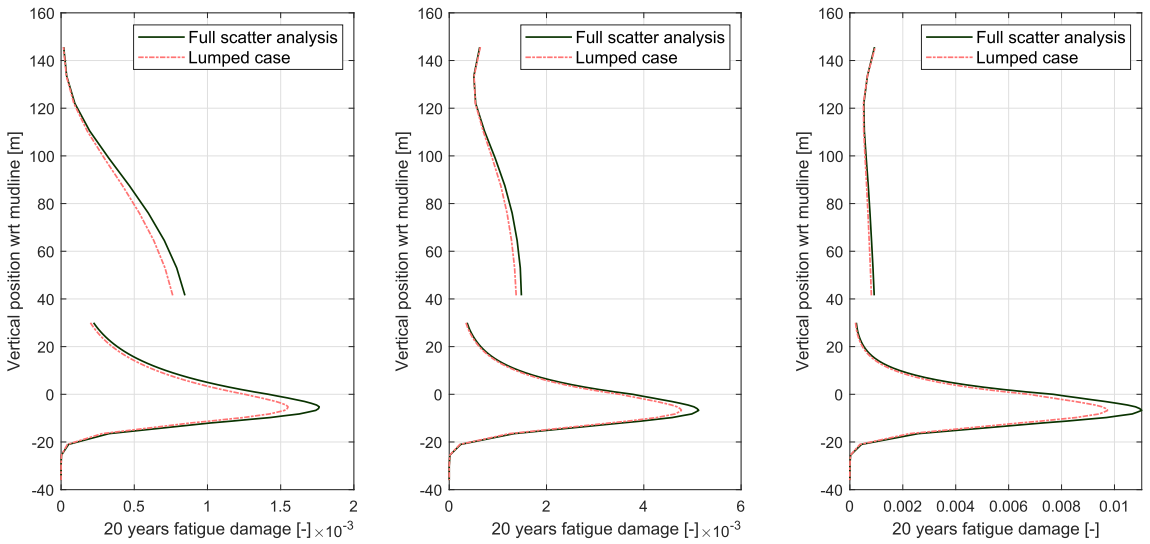

(a) Wind class 6-8 m/s (b) Wind class 12-14 m/s (c) Wind class 18-20 m/s

Fig. 21. Lifetime fatigue damage from full scatter diagram and lumped load cases with 30° wind-wave misalignment.

position on both the tower and monopile. In the two other wind speed classes, the error is 10–12% at the most critical positions.

These errors are larger than those seen for aligned wind and waves. However, the corresponding error in damage equivalent stress is 2.3% or lower for all cases. This is similar to the uncertainty introduced by the thickness tolerance for tower and monopile walls, as reported in Ref. [37].

5.5. Fatigue damage sensitivity to lumped load cases

The sensitivity of the fatigue damage to variation in H_s and T_p is evaluated for three wind speed classes; 8–10 m/s, 12–14 m/s, and 18–20 m/s. Each parameter is varied around its nominal value (i.e. the FLDC value from Table 6) with a factor between 0.6 and 1.4, while the other parameter is kept constant. All the $H_s - T_p$ combinations of the modified load cases are within the wave steepness limits suggested by the design codes [30]. The average 1-hr fatigue damage from 10 realisations is compared. The sensitivity is expressed as

the ratio between the damage of the modified load cases to the damage from the nominal lumped load case. An example of damage sensitivity to $H_s - T_p$ is shown in Fig. 22 for two wind speed classes, and for different locations along the support structure. The bottom and top x-axis show the normalised and actual parameter values, respectively. The results are similar for all three wind classes.

Fig. 22a clearly indicates that for locations on the tower and close to the sea surface, there is an approximately linear variation of the fatigue damage with respect to H_s. As the moment arm increases for locations deeper along the monopile and closer to mudline, the relation between H_s and fatigue damage variation gradually approaches to follow H_s^4. This is lower than the theoretical limit for wave-only loads, where the fatigue damage would follow H_s^5 [7,29]. The lower exponent reflects that wind-induced loads also contribute to the fatigue damage, which decreases the sensitivity to wave loads.

Fig. 22b indicates that the influence of T_p variation to fatigue damage is similar along the support structure, given that T_p is sufficiently far from the natural period of the structure. For longer wave periods, the response becomes more quasi-static, reducing the number of load cycles. As a result, fatigue damage is steadily decreased, with slight variations along the support structure. The opposite effect is observed by decreasing the T_p. However, when approaching the natural period range (i.e. 3.7–4.0 s), the effect of T_p variation is pronounced due to the high dynamic amplification. The effect is more significant for the tower and monopile locations close to sea surface as the relative deflections in the first mode shape are larger there than i.e. at mudline. The sensitivity seen for variations in T_p corresponds well with T_p^{-1}. This is the theoretical curve obtained for wave-only loads if it is assumed that changes in T_p only affect the number of load cycles [7]. A steeper curve is obtained if changes in wave kinematics are taken into account, with the limit T_p^{-11} for a narrow-banded wave spectrum [29]. As for H_s, the true curve approaches T_p^{-1} since the wind loads reduce the sensitivity to wave loads.

If it is desirable to modify the sea-state parameters of the lumped load cases (i.e. to get less or more conservative fatigue damage values), it is recommended to change the T_p value, ensuring that it has sufficient distance from the natural period. This is due to the fact that T_p variations affect the different locations in tower and monopile more similarly. In contrast, H_s variations affect the locations with large moment arm (i.e. close to mudline) more significantly than locations close to sea surface and the tower.

5.6. *Lumped load cases selection sensitivity in foundation design changes*

The penetration depth is one of the most important design parameters for monopile foundations from safety and economical perspective. The frequency-domain lumping method for aligned wind and waves, was applied to the other four foundation models (subsection 3.2.2), which vary in penetration depth. The purpose was to evaluate the lumped load case selection sensitivity on foundation design variations. Fig. 23 shows the contour lines for wind speed class 18–20 m/s for two foundation models at mudline and tower base.

Contour lines are similar also for the rest of the models. Slight differences of the dynamic properties of the models (Fig. 9) affected the contour lines only in the natural period range of the structure, while for T_p larger than 4.5 s the contour lines are identical. The same is observed for all wind speed classes. This resulted in identical lumped load cases for all wind speed classes, as illustrated in Fig. 23 where the selected $H_s - T_p$ combinations for each class are shown. As a result, the same lumped load cases can be used for different designs with good accuracy as long as T_p of the lumped load case is far enough away from the OWT natural period.

6. Conclusion

In this paper two environmental lumping methods were investigated based on the damage-equivalent contour lines approach. The DTU 10 MW reference wind turbine supported on a monopile foundation is used for the study. The aim of both methods is to condense

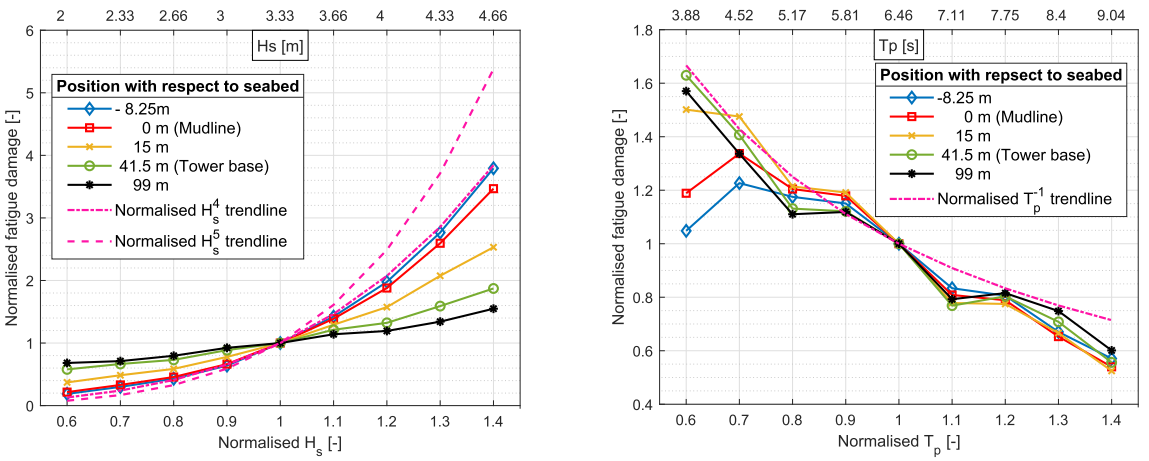

(a) H_s sensitivity (Wind class 18-20 m/s) (b) T_p sensitivity (Wind class 12-14 m/s)

Fig. 22. Normalised fatigue damage sensitivity for various locations along the support structure as function of H_s, T_p variation.

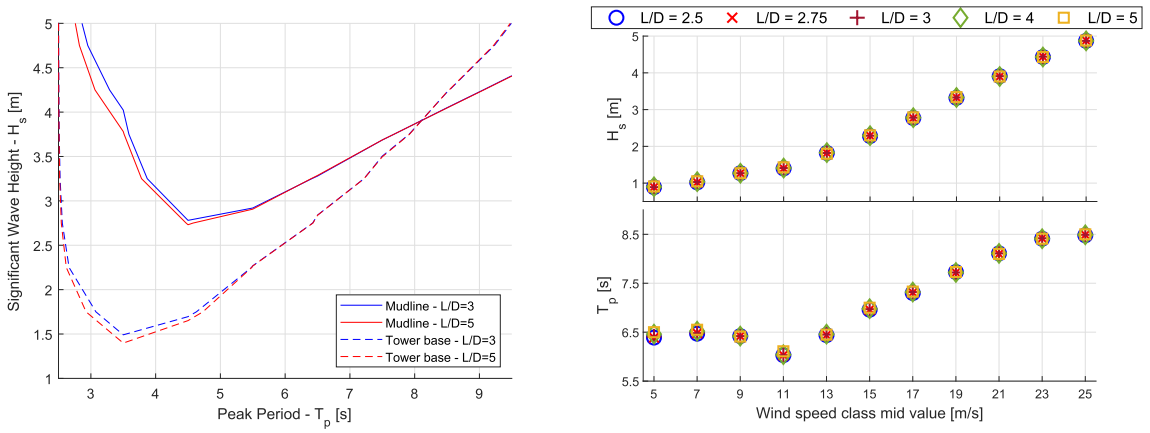

(a) Contour lines (b) Lumped $H_s - T_p$

Fig. 23. (a) Contour lines of two foundation models from frequency-domain lumping method for wind speed class 18–20 m/s (b) Lumped sea-state parameters of each foundation model per wind speed class.

each scatter diagram associated with a wind speed class to a single sea-state load case. The frequency-domain method uses a transfer function from wave elevation to stress, to determine the contour lines and resultant lumped load cases. Stress transfer functions are extracted from a 3-hr white-noise wave excitation and uniform wind for a given scatter diagram. The time-domain approach is based on time-domain simulations, it is only used for comparison to frequency-domain method and not as an alternative to full scatter analysis.

The wind turbine operational range was considered, including 11 wind speed classes, each one associated with a sea-state scatter diagram. Selected lumped load cases are subjected to simultaneous wind-wave loads to predict long-term fatigue damage. The accuracy of the damage estimate varied between ±13% for individual wind speed classes with a maximum difference of ∼6% for the total fatigue damage compared to full scatter fatigue assessment. These differences are considered to be acceptable notably in view of the significant improvement in computational efficiency (∼93%); 55 1-hr time-domain simulations (5 for each lumped load case to reduce statistical uncertainty) have been conducted for a reduced load set instead of 800 (full scatter analysis). Furthermore, these differences are tolerable considering the inherent uncertainty of condensing a scatter diagram in one load case, the uncertainty in fatigue damage estimation per 1-hr simulation and the nonlinearities in the environmental models. Similar accuracy is found for aligned wind-waves with and without considering long-term wind direction variability. It is recommended to validate this in sites with different environmental databases.

Using several contour lines for the selection of lumped load cases ensured preservation of fatigue damage with the same level of accuracy in the whole support structure, compared to the full scatter results. The fatigue damage sensitivity to H_s and T_p variations was also evaluated. As long as the nominal T_p value is far from the natural period, variations of ∼10% result in fairly uniform change in the damage along the support structure. However, similar changes in H_s lead to significant damage differences (∼40%) for locations with large moment arm (i.e. close to mudline), while locations close to sea-surface and the tower are much less affected (∼10%). For wind-wave misalignment cases, an underestimation of approximately 10% was observed in fatigue damage for the evaluated wind speed classes. Taking into account the considerable reduction in computational effort, this error might be acceptable in an early design stage.

Lumped load cases from frequency-domain lumping method were compared for five monopile designs of different penetration depth, with L/D ratio varying from 2.5 to 5. For the system being considered, the dynamic properties were insensitive to the penetration length, such that the resulting lumped cases did not change significantly. This is useful, as design changes are expected during the design optimisation process, but this should be examined for other structural parameters, such as monopile diameter or thickness, where larger changes in the natural period may be expected.

Declaration of competing interest

The authors declare that they have no known competing financial interests or personal relationships that could have appeared to influence the work reported in this paper.

Acknowledgements

The authors gratefully acknowledge the support from the Wave Loads and Soil Support for Extra Large Monopiles (WAS-XL) project (NFR grant 268182). Additionally, part of this work has been carried out at the Centre for Autonomous Marine Operations and Systems (AMOS). The Norwegian Research Council is acknowledged as the main sponsor of NTNU AMOS. This work was supported by the Research Council of Norway through the Centres of Excellence funding scheme, project number 223254 - AMOS. The authors gratefully appreciate the collaboration and discussions with Ana Page from NGI during the study.

References

[1] Selot F, Fraile D, Brindley G. Offshore wind in Europe - key trends and statistics, Published in February 2020, WindEurope. Tech. rep; 2020.
[2] Hermans JM, Peeringa KW. Future XL monopile foundation design for a 10MW wind turbine in deep water. Tech. rep; December, 2016. ECN-E–16-069.
[3] ABS (American Bureau of Shipping). Guide for the fatigue assessment of offshore structures. 2014.
[4] DNV-GL (Det Norske Veritas - Germanischer Lloyd), Fatigue design of offshore steel structures (DNVGL-RP-C203).
[5] Du J, Chang A, Wang S, Li H. A novel lumping block method for fatigue damage assessment of mooring chain. 2014.
[6] DNV-GL (Det Norske Veritas - Germanischer Lloyd). Riser fatigue. 2017 (DNVGL-RP-F204).
[7] Kühn M. Dynamics and design optimisation of offshore wind energy Conversion systems. Ph.D. Thesis. Delft, The Netherlands: Technische Universiteit Delft; 2001. ISBN 90-76468-07-9.
[8] M. Seidel, Wave induced fatigue loads - insights from frequency domain calculations, Stahlbau 83. doi:10.1002/stab.201410184.
[9] Seidel M. Wave induced fatigue loads on monopiles - new approaches for lumping of scatter tables and site specific interpolation of fatigue loads. In: International wind engineering conference. IWEC; 2014.
[10] IEC (International Electrotechnical Commission). Design Requirements of offshore wind turbines. 2009 (IEC 61400-3).
[11] DNV-GL (Det Norske Veritas - Germanischer Lloyd). Support structures for wind turbines. 2016 (DNVGL-ST-0126).
[12] Passon P, Branner K. Condensation of long-term wave climates for the fatigue design of hydrodynamically sensitive offshore wind turbine support structures. Ships Offshore Struct 2014;11:142–66.
[13] Jenkins N, Burton A, Sharpe D, Bossanyi E. Wind energy handbook. John Wiley and Sons Ltd; 2001.
[14] Passon P. Damage equivalent wind-wave correlations on basis of damage contour lines for the fatigue design of offshore wind turbines. Renew Energy 2015;81:723–36.
[15] Jonkman J, Butterfield S, Musial W, Scott G. Definition of a 5-mw reference wind turbine for offshore system development. Report NREL/TP-500-38060; TRN: US200906US200906CO (United States) (2009). URL, https://www.osti.gov/servlets/purl/947422.
[16] Carroll J, McDonald A, Dinwoodie I, McMillan D, Revie M, Lazakis I. Availability, operation and maintenance costs of offshore wind turbines with different drive train configurations. Wind Energy 2017;20(2):361–78. https://doi.org/10.1002/we.2011.
[17] Page A, Grimstad G, Eiksund G, Jostad HP. A macro-element pile foundation model for integrated analyses of monopile based offshore wind turbines. Ocean Eng 2018;167:23–35.
[18] MacCamy RC, Fuchs RA. Wave forces on piles: a diffraction theory. Tech. Memo No. 69, U.S. Army Corps of Engrs; 1954.
[19] Barltrop NDP, Adams AJ. Dynamics of fixed marine structures. third ed. Oxford: Butterworth-Heinemann; 1991.
[20] Dirlik T. Application of computers in fatigue analysis, Phd thesis. 1985. http://wrap.warwick.ac.uk/2949/.
[21] Li L, Gao Z, Moan T. Joint environmental data at five European offshore sites for design of combined wind and wave energy devices. In: International conference on ocean, offshore and arctic engineering. OMAE; 2013.
[22] Bak C, Zahle F, Bitsche R, Kim T, Yde A, Henriksen LC, et al. Description of the DTU 10 MW reference wind turbine. Tech. rep., Technical University of Denmark, Department of Wind Energy; 2013.
[23] Jonkman BJ. TurbSim user's guide: version 1.50, technical report. Tech. rep; 2009. NREL/TP-500-39797, National Renewable Energy Laboratory.
[24] Burton T, Jenkins N, Sharpe D, Bossanyi E. Wind energy handbook. John Wiley & Sons, Ltd; 2011.
[25] Bachynski E, Ormberg H. Comparison of engineering models for the aerodynamic load distribution along a wind turbine blade 2015. 2015. p. 561–7.
[26] Correia A. A pile-head macro-element approach to seismic design of monoshaft supported bridges. 2011. Ph.D. thesis, Pavia, Italy.
[27] Page A, Grimstad G, Eiksund G, Jostad HP. A macro-element model for multidirectional cyclic lateral loading of monopiles in clay. Comput Geotech 2019;106:314–26.
[28] Grimstad G, Andresen L, Jostad HP. Ngi-adp: anisotropic shear strength model for clay. Int J Numer Anal Methods GeoMech 2012;36(4):483–97. https://doi.org/10.1002/nag.1016.
[29] Velarde J, Bachynski EE. In: Design and fatigue analysis of monopile foundations to support the DTU 10 MW offshore wind turbine, vol. 137. Energy Procedia; 2017. p. 3–13.
[30] DNV-GL (Det Norske Veritas - Germanischer Lloyd). Environmental conditions and environmental loads. 2017 (DNVGL-RP-C205).
[31] Matsuishi M, Endo T. Fatigue of metals subjected to varying stress. In: Kyushu branch of jpan society of mechanics engineering; 1968. p. 37–40.
[32] Brodtkorb P, Johannesson P, Lindgren G, Rychlik I, Ryden J, Sjo E. WAFO—a MATLAB Toolbox for the analysis of random waves and loads. In: 10th international offshore and polar engineering conference (ISOPE), vol. 3; 2000. p. 343–50.
[33] Bachynski EE, Kvittem MI, Luan C, Moan T. Wind-wave misalignment effects on floating wind turbines: motions and tower load effects. J Offshore Mech Arctic Eng 2014;136.
[34] Horn JT, Bitner-Gregersen EM, Krokstad J, Leira B, Amdahl J. A new combination of conditional environmental distributions. Appl Ocean Res 2018;73:17–26.
[35] Katsikogiannis G, Bachynski EE, Page AM. Fatigue sensitivity to foundation modelling in different operational states for the DTU 10 MW monopile-based offshore wind turbine. J Phys Conf 2019;1356:012019.
[36] Damgaard M, Ibsen LB, Andersen LV, Andersen J. Cross-wind modal properties of offshore wind turbines identified by full scale testing. Wind Engineering & Industrial Aerodynamics 2013;116:94–108.
[37] Velarde J, Kramhøft C, Sørensen JD. Global sensitivity analysis of offshore wind turbine foundation fatigue loads. Renew Energy 2019;140:177–89. https://doi.org/10.1016/j.renene.2019.03.055.